Computationally Guided Design of Single-Chain Variable Fragment Improves Specificity of Chimeric Antigen Receptors

Andrey Krokhotin,[1,6] Hongwei Du,[2,6] Koichi Hirabayashi,[2] Konstantin Popov,[1] Tomohiro Kurokawa,[3] Xinhui Wan,[3] Soldano Ferrone,[3] Gianpietro Dotti,[2,4] and Nikolay V. Dokholyan[5]

[1]Department of Biochemistry and Biophysics, University of North Carolina at Chapel Hill, Chapel Hill, NC 27599, USA; [2]Lineberger Cancer Center, University of North Carolina at Chapel Hill, Chapel Hill, NC 27599, USA; [3]Department of Surgery, Massachusetts General Hospital, Harvard Medical School, Boston, MA, USA; [4]Department of Microbiology and Immunology, School of Medicine, University of North Carolina, Chapel Hill, NC 27599, USA; [5]Departments of Pharmacology and Biochemistry & Molecular Biology, Penn State College of Medicine, Hershey, PA 17033, USA

Chimeric antigen receptor (CAR)-T cell-based immunotherapy of malignant disease relies on the specificity and association constant of single-chain variable fragments (scFvs). The latter are synthesized from parent antibodies by fusing their light (V_L) and heavy (V_H)-chain variable domains into a single chain using a flexible linker peptide. The fusion of V_L and V_H domains can distort their relative orientation, thereby compromising specificity and association constant of scFv, and reducing the lytic efficacy of CAR-T cells. Here, we circumvent the complications of domains' fusion by designing scFv mutants that stabilize interaction between scFv and its target, thereby rescuing scFv efficacy. We employ an iterative approach, based on structural modeling and mutagenesis driven by computational protein design. To demonstrate the power of this approach, we use the scFv derived from an antibody specific to a human leukocyte antigen A2 (HLA-A2)-HER2-derived peptide complex. Whereas the parental antibody is highly specific to its target, the scFv showed reduced specificity. Using our approach, we design mutations into scFvs that restore specificity of the original antibody.

INTRODUCTION

Single-chain variable fragments (scFvs), obtained from antibodies by connecting their light (V_L) and heavy (V_H)-chain domains with a peptide flexible linker, allow harnessing specificity of antibodies in a conceptually simpler single-chain construct. scFvs are generally used in phage display,[1] flow cytometry, immunohistochemistry, and more recently, in generating chimeric antigen receptors (CARs) in which the scFv is fused with T cell signaling molecules to redirect the antigen specificity of T lymphocytes.[2,3] Despite successful applications of scFv in CAR-T, the specificity and the association constant of the scFvs do not always match those of the parent antibody, because rewiring the connectivity of V_L and V_H chain domains of the parent antibody can change their dynamics and relative orientation.

To demonstrate this complication in constructing scFv, we selected an antibody that recognizes a peptide processed and presented physiolog-ically into the grove of the human leukocyte antigen A2 (HLA-A2) complex, reasoning that even small distortions of the antibody structure in a scFv format may alter the recognition of the peptide/HLA complex because of the high specificity of the peptide/HLA interaction. We developed an antibody (SF2) specific to the HLA-A2/peptide complex in which the KIFGSLAFL peptide derives from the human HER2 protein. The SF2 antibody shows no binding toward the empty HLA-A2 complex, whereas the binding to the HLA-A2/KIFGSLAFL peptide complex is typically peptide concentration dependent (Figure S1). We then cloned the V_H and V_L chains of the SF2 antibody and generated a scFv by connecting the C terminus of V_L with the N terminus of V_H via a Gly-Ser linker. This scFv was then fused with the hinge and transmembrane domain of CD8α and endodomains of CD28 and CD3ζ to generate the CAR (SF2.CAR) (Figure S2A). Retroviral particles encoding the SF2.CAR were used to generate SF2.CAR-expressing T cells (SF2.CAR-Ts) using previously validated protocols to generate CAR-T cells for clinical use (Figures S2B and S2C).[4] Surprisingly, SF2.CAR-T cells displayed activity not only toward T2 cells loaded with the HER2 KIFGSLAFL peptide, but also against empty T2 cells and T2 cells loaded with an irrelevant peptide as assessed by interferon gamma (IFNγ) release assay (Figure S2D), indicating that the scFv conformation or its assembling in the CAR format substantially modify the specificity of the parental SF2 antibody.

We argued that by mutating key residues in the binding interface between scFv and the HLA-A2/peptide complex, we can restore specificity of scFv toward the target HER2 peptide. This approach requires knowledge of the complex tertiary structure. Traditional methods of tertiary

structure determination such as X-ray crystallography or cryo-electron microscopy are technically challenging and provide only a static snapshot of the structure. NMR can be used to explore structure dynamics, but protein size is a limiting factor for the NMR applicability. Computational modeling provides an alternative to experimental approaches and allows to predict structure and explore its dynamics. However, due to inaccuracies present in modern force fields, computational modeling cannot unambiguously identify the correct structure but can provide a range of alternative models. To validate the model of scFv bound to the HLA-A2/peptide complex, we generated a set of scFv mutants. We developed an empirical scoring function, which allowed us to rank computational models based on comparison between predicted and experimentally measured effects, which these mutants exert on binding between scFv and the HLA-A2/peptide complex. The top-ranked models were selected and evaluated using an additional set of mutants. By following this iterative modeling and redesign procedure, we determined the structure of scFv complexed with HLA-A2 loaded with the HER-2 peptide, and identified mutations that improve the binding specificity of the scFv in the CAR format.

RESULTS

Probing Structure of scFv Bound to the HLA-A2/KIFGSLAFL Peptide Complex

The computational methods used for prediction of antibody structure have gradually improved over the last decade as revealed by the Antibody Modeling Assessment, a community-wide competition aimed to evaluate performance of antibody modeling software.[5,6] The best models match experimental structures with angstrom accuracy even for the hardest to predict, the third complementarity-determining region (CDR) of the V_H variable domain.[7] To predict the tertiary structure of the SF2 antibody, we used antibody modeling software.[8] The corresponding scFv is obtained by connecting the C terminus of V_L to the N terminus of V_H by $(GGGGS)_3$ linker. To explore dynamics of these structures, we ran discrete molecular dynamics (DMD) simulations[9–11] (Materials and Methods). We found that although the mutual orientation of V_L and V_H is the same both in antibody and scFv, scFv exhibits higher fluctuations, as revealed by the distribution of root-mean-square fluctuations (RMSFs) (Figure 1; Videos S1 and S2). Thus, increased flexibility of the scFv, as compared with the SF2 antibody, affects specificity of the scFv. We argue that we can restore the specificity of the scFv by introducing mutations that stabilize it on substrate, thereby decreasing its flexibility.

We used template structure (PDB: 1HHI) to model HLA-A2/peptide (Materials and Methods). To infer binding pose of scFv to the HLA-A2/peptide complex, we used docking software.[12,13] After discarding apparently inconsistent models (Figure 2B), where none of the six complementarity-determining regions (CDRs) of the scFv binds the HER2 peptide, we obtained 270 3D models. We then clustered these models (Figure 2C) and identified eight distinct clusters (Figure S3). For each cluster we chose a centroid structure as a representative model. For each residue within CDRs of representative models, we considered all possible mutations and calculated: (1) change in stability of the scFv/HLA-A2/peptide complex upon mutation; (2) change in the interaction energy between scFv and peptide; and (3) change in the interaction energy between scFv and HLA-A2 (Materials and Methods). We selected a set of six mutations in V_H and six mutations in V_L domains (named set I) for further experimental probing. The selected mutations stabilize the interaction between scFv and peptide relatively to the interaction between the antibody and HLA-A2 complex in more than one considered model.

We validated these mutations by generating mutant SF2.CAR molecules, constructing CAR-T cells for each specific mutant, and testing their specific activity. For this purpose, we measured IFNγ release by CAR-T cells co-cultured with T2 cells loaded with the specific HER2-$P_{369-377}$ peptide or with the irrelevant MAGEA3-$P_{271-279}$ peptide or not loaded with any peptide (Figure S4). The results showed that the mutations V_L-S31Y, V_L-G93L, and V_H-G55F did not affect the specific binding to HER2-$P_{369-377}$ peptide-loaded HLA-A2 molecules but decreased the binding to irrelevant MAGEA3-$P_{271-279}$ peptide-loaded HLA-A2 molecules and to empty HLA-A2 molecules.

For each computational model we calculated the scoring function in order to assess compatibility of the model and experimental data (Figure 2D) (Materials and Methods). The scoring function is a sum of scores over all experimentally tested mutations and consists of two terms. In the first term the theoretically calculated change in global stability of the HLA-A2/peptide-antibody complex ($\Delta\Delta G^{TH}$) is compared with the approximate value derived from experimental data ($\Delta\Delta G^{EXP}$). In the second term the relative stabilization of interaction between scFv and peptide versus interaction between scFv and HLA-A2 is calculated theoretically ($\Delta E_{pep-HLA-Ab}^{TH}$) and compared with the approximate value derived from experimental data ($\Delta E_{pep-HLA-Ab}^{EXP}$). The model with minimal score corresponds to the model best matching the experimental data.
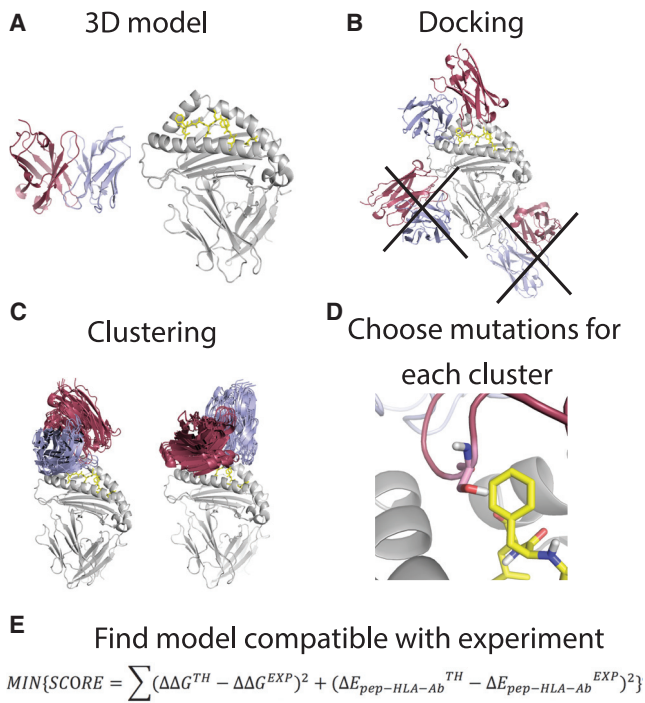
A 3D model

B Docking

C Clustering

D Choose mutations for each cluster

E Find model compatible with experiment

$$MIN\{SCORE = \sum (\Delta\Delta G^{TH} - \Delta\Delta G^{EXP})^2 + (\Delta E_{pep-HLA-Ab}{}^{TH} - \Delta E_{pep-HLA-Ab}{}^{EXP})^2\}$$

Figure 2. Structure Prediction Workflow

(A) Structural models are created for scFv and HLA-A2 molecule loaded with HER2-derived peptide. (B) Computation docking of scFv to the HLA-A2/peptide complex. Models, where scFvs do not touch peptide, are discarded. (C) Clustering of derived models. (D) Residues in the CDRs of scFvs are explored for the effect of their mutations on the centroids of the clusters from step (C). (E) The models most compatible with predictions are further selected and clustered with a smaller cutoff. New mutations are proposed.

It is noteworthy that choice of initial mutations is not unique, and alternative sets can be used instead. However, our choice of initial set based on stabilization of antibody/peptide interaction in some of the models allows us in case of success to obtain correct mutations already with the first set of experiments. After ranking models using our scoring function, we selected the top 10 models (out of 270 initial models). For these models we selected a new set of best matching mutations (named set II) that consists of seven mutations in total. CAR-T cells expressing these new SF2.CAR mutants were generated, and their function was tested by the co-culture experiment and IFNγ release assay (Figure S5). We find that the mutations S53M and S100V increased binding to HER2-P$_{369-377}$ peptide-loaded HLA-A2 molecules but decreased the binding to irrelevant MAGEA3-P$_{271-279}$ peptide-loaded HLA-A2 molecules and to empty HLA-A2 molecules.

The functional characterization of the new scFv mutations of set II, along with the best mutations from set I, was further validated with CAR-T cells generated from multiple donors and illustrated in Figure 3. They were evaluated using our scoring function. Based on these results, we selected the model with the lowest scoring function (Figure 4A).

Assessment of the Model Quality

The selected model correctly describes most of the mutations from sets I and II. Three mutations from set I (V$_L$ S31Y, V$_L$ G93L, and V$_H$ G55F) exhibited decrease in binding affinity to both empty and peptide-loaded HLA-A2 complex (Figure S4). Based on our model, we predict that upon these mutations, large hydrophobic residues become exposed to the solvent (Figures 4B–4D), thus decreasing overall stability of the complex. Two mutations from set II (V$_H$ S100V and V$_H$ S53M) (Figures 4E and 4F) preserved binding affinity of the scFv to peptide-loaded HLA-A2, whereas drastically reducing binding to the empty HLA-A2 complex (Figure S5). In line with this observation, our model suggested that these residues directly interact with F8 residue of the peptide, which provides an anchor for successful recognition of the peptide by the scFv. These mutations increase contact surface between F8 and the scFv, thus increasing the energy of van der Waals interactions.

The developed structural model also explains differential effects of the A50 mutations, such that A50L completely abrogates the interaction between scFv and the HLA-A2 complex, whereas A50V conserves some residual binding, and A50F preserves the binding but reduces its specificity. According to our model, A50L and A50V mutations result in clashes with the HLA-A2 H1 helix, whereas A50F mutation rests on top of the H1 helix without clashes (Figure S6). Furthermore, interaction between A50F mutation and H1 helix increases the binding between scFv and the empty HLA-A2 complex, causing reduced specificity for the interaction with the peptide.

We also compared binding pose of the scFv as inferred from the modeling to the orientation of typical T cell receptor (TCR) bound to the HLA-A2/peptide complex (Figure S7). At least 50 unique TCR-peptide-major histocompatibility complex (MHC) class I complexes with 3D structures have been deposited into the PDB. All of them follow the classical binding pattern of TCR[14] with a few exceptions where TCR orientation is flipped by 180°.[15] A typical TCR binds the MHC complex in the gap between H1 and H2 helices, thus maximizing interaction with a peptide and minimizing non-specific interaction with empty MHC. The interaction with the peptide is mediated by CDR3 loops, whereas germline-encoded CDR1 and CDR2 loops mostly contact MHC H1 and H2 helices.[14,16] In our model, scFv accommodates a different binding pose. We observed that contact between scFv and peptide is mediated by H2 and H3 CDR loops. V$_L$ does not bind the peptide but makes extensive contact to MHC walls. This structure explains the high non-specific binding of the wild-type scFv.

DISCUSSION

Here, we presented a novel approach for optimization of binding specificity of scFv. It relies on structural modeling and mutagenesis, and does not require prior knowledge of antibody 3D structure. We validated our approach on the scFv derived from an antibody specific to the KIFGSLAFL peptide loaded into the HLA-A2 complex. We built a model of the complex that captures fine structural details, such that it can explain the differences in binding of scFv to the
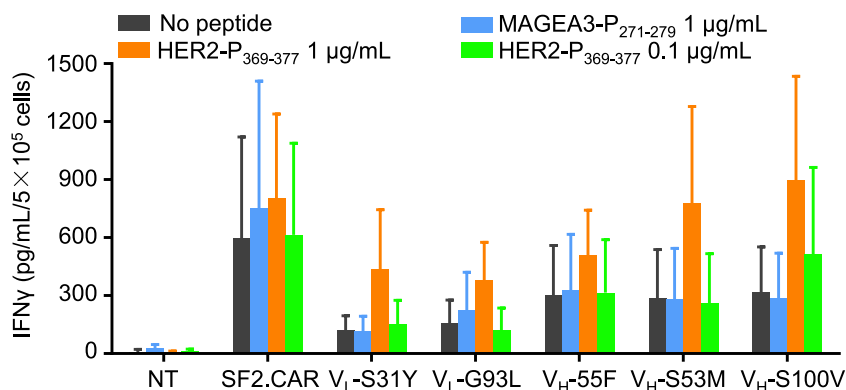
Figure 3. IFNγ Release by SF2.CAR Mutants

Control T cells (NTs), SF2.CAR-T cells, and T cells expressing the CARs generated with the mutant scFvs were cultured for 24 h with empty T2 cells or with T2 cells loaded with the KIFGSLAFL (HER2$_{369-377}$) peptide or an irrelevant peptide (MAGEA3$_{271-279}$). All T cells expressing the CAR were normalized for CAR expression. IFNγ level released in the supernatant was measured by ELISA in the supernatant harvested following a 24-h incubation. The results are average ± SD of four experiments.

HLA-A2/peptide complex when the same residue is mutated to different amino acids.

We found that the scFv is more flexible than parental SF2 antibody. We also predicted that binding pose of the scFv on the top of the HLA-A2/peptide complex differs from what is expected based on comparison with TCR binding. These two observations together can explain non-specific binding observed for the wild-type scFv. We established two mutations that reduce non-specific binding, while preserving binding to peptide loaded to the HLA-A2 complex at the same level.

An interesting avenue to explore is possible allosteric effects, which mutations exhibit on binding interface between scFv and the HLA-A2/peptide complex. The phenomenon of allostery, which refers to the process when perturbation of one site within a macromolecule affects another distant site, attracts broad attention.[17–19] In particular, loop regions are shown to be important for propagation of allosteric effects,[20] which suggests potential importance of CDR loops in allosteric modulation of antigen binding. It was previously shown that mutations can trigger allosteric modulations of antibody[21] and scFv.[22] To reveal allosteric effects within our system, we used the AlloSigMA server[23] (Materials and Methods). Interestingly, we found changes in protein dynamics far away from mutation sites (Figure S8), which reveals allosteric modulation of binding between scFv and the HLA-A2/peptide complex.

In the current manuscript we use standard (GGGGS)$_3$ linker to connect V$_L$ and V$_H$ chain variable domains into scFv. Optimization of the linker length and composition can be used to further improve specificity of scFv. It was previously shown that lengthening of (GGGGS)$_n$ linker can increase activity of scFv toward corresponding antigen,[24] whereas shortening of the linker can destabilize interaction of V$_L$ and V$_H$ within a single scFv and leads to multimerization of scFv.[25]

Although antibodies can be derived to bind peptide inserted into the MHC complex, their sequence is not optimized for minimization of non-specific binding to the MHC complex as it is in the case of TCRs, which evolved complementarity to MHC during millions

of years of evolution. Optimizing antibody design using sequence snippets of the α- and β-chains of TCR may improve low non-specific binding affinity of TCRs.

There is a significant demand of finding an efficient way to optimize the affinity of the scFv in CAR molecules with the goal to select and maintain high specificity for antigens expressed at high levels in tumor cells, but also expressed at low levels in some normal tissues. Our proposed computational model can also be adapted to tune the affinity of the scFv to minimize on target but out of tumor activity.

MATERIALS AND METHODS
Structure Modeling and Model Selection Workflow
The 3D structure of the SF2 antibody was built using the Kotai web server.[8] In total, 21 models of antibody, which differ in the conformation of the third complementarity-determining regions of a V$_H$ variable domain (CDR H3), are considered (Figure 2A). HLA-A2 structure is built based on the template structure (PDB: 1HHI), where we replace the original peptide by the HER2 peptide. For that we kept peptide backbone geometry intact and replaced corresponding side chains. We verified that anchor residues (positions 2, 6, and 9)[26] point inward HLA-A2. The initial structure was run through short DMD simulation to release inter-atomic clashes. The simulation was run for 10,000 steps at T = 0.5 kcal/(mol·k$_B$) with heat exchange coefficient = 10. The Andersen thermostat is used.[27]

DMD simulations for the RMSF plot were performed for 1 million steps at T = 0.55 kcal/(mol k$_B$) with heat exchange coefficient = 0.1. In total, five trajectories for SF2 antibody and five trajectories for the scFv form of the antibody were produced. RMSF is calculated over carbon-alpha atoms of the protein backbones.

Docking was performed with the ClusPro[13] web server, resulting in 598 models in total (Figure 2B). The structure used for docking contains V$_H$ and V$_L$ variable domains without the Gly-Ser linker. After discarding apparently incorrect models, where none of the six complementarity-determining regions (CDRs) of antibodies touch the HER2 peptide, we got 270 3D models. The resulting models were run through DMD simulations [10,000 steps,
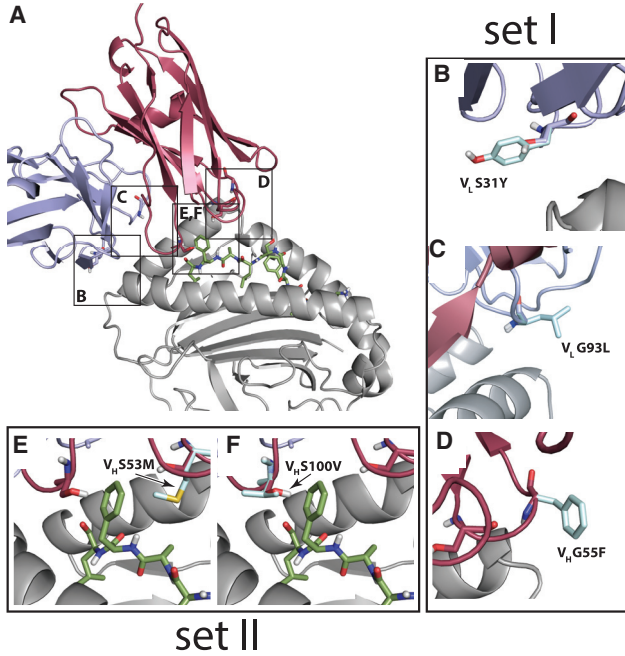
Figure 4. Structural Model Best Matching Mutagenesis Data

(A) scFv bound to the HLA-A2/KIFGSLAFL peptide complex. Black boxes highlight location of five residues, which increase specificity of scFv toward the target peptide upon specific mutation. (A–F) The mutants (B) V_L S31Y, (C) V_L G93L, (D) V_H G55F, (E) V_H S53M, and (F) V_H S100V are shown. These mutations were performed at two sets of experiments (set I and set II). V_L is colored in light blue; V_H is colored in magenta. The mutated residues are colored in cyan.

T = 0.5 kcal/(mol·k_B), heat exchange coefficient = 10]. The models were aligned in 3D space using the position of HLA-A2 and clustered by root-mean-square deviation (RMSD) of carbon-alpha backbone atoms of antibodies (Figure 2C), which gave eight distinct clusters (Figure S3). Clustering cutoff distance is 9 Å. The clusters were counted if the number of structures in the cluster is ≥10.

We identified CDRs using a previously described set of rules.[28] For each structure representing centroid of clusters and for each CDR residue (61 residues in total) we determined the effect of every possible mutation (Figure 2D). For that we calculate: (1) change of HLA-A2/peptide-antibody complex stability upon the mutation (ΔΔG); (2) change of interaction energy between antibody and HLA-A2 (ΔE_{HLA-Ab}); and (3) change of interaction energy between antibody and peptide (ΔE_{pep-Ab}). The change of stability is calculated using Eris software package in the scanning mode.[29,30] The interaction energies are calculated using a software toolkit based on DMD[10] and Medusa force field.[31,32] For experimental testing we selected mutations that stabilize interactions between antibody and peptide as compared with the interaction between antibody and HLA-A2 (ΔΔG < 1.5 and $\Delta E_{pep-Ab} - \Delta E_{HLA-Ab} < -1$).

The models are checked for consistency with experimental data. For that we define empirical energy function:

$$SCORE = \sum \left(\Delta\Delta G^{TH} - \Delta\Delta G^{EXP} \right)^2 + \left(\Delta E^{TH}_{pep-HLA-Ab} - \Delta E^{EXP}_{pep-HLA-Ab} \right)^2 \quad \text{(Equation 1)}$$

where sum is calculated over all experimentally tested mutations for each model

$$\Delta\Delta G^{TH} = \begin{cases} -1 & if\ x < -1 \\ x & if\ -1 < x < 1 \\ 1 & if\ x > 1 \end{cases}$$

$x = \Delta\Delta G / E_{thresh}$ and $E_{thresh} = 4 kcal/mol$ is an empirically derived threshold. The mutations with $\Delta\Delta G$ exceeding this threshold severely affect protein stability.

$$\Delta\Delta G^{EXP} = \begin{cases} -1 & if\ y < -1 \\ y & if\ y > -1 \end{cases}$$

$y = (IFN\gamma^{WT}_{HLA-pep} - IFN\gamma^{MUT}_{HLA-pep}) / IFN\gamma^{WT}_{HLA-pep}$, where $IFN\gamma^{WT}_{HLA-pep}$ and $IFN\gamma^{MUT}_{HLA-pep}$ define interferon gamma response as measured by ELISA assay for the wild-type and mutated antibodies against the HLA-A2/peptide complex.

$$\Delta E^{TH}_{pep-HLA-Ab} = \begin{cases} -1 & if\ z < -1 \\ z & if\ -1 < z < 1 \\ 1 & if\ z > 1 \end{cases}$$

$z = (\Delta E_{pep-Ab} - \Delta E_{HLA-Ab}) / E_{thresh}$

$$\Delta E^{EXP}_{pep-HLA-Ab} = \begin{cases} -1 & if\ w < -1 \\ w & if\ -1 < w < 1 \\ 1 & if\ w > 1 \end{cases}$$

$w = \dfrac{(IFN\gamma^{WT}_{HLA-pep} - IFN\gamma^{WT}_{HLA}) - (IFN\gamma^{MUT}_{HLA-pep} - IFN\gamma^{MUT}_{HLA})}{(IFN\gamma^{WT}_{HLA-pep} - IFN\gamma^{WT}_{HLA})}$, where $IFN\gamma^{WT}_{HLA}$ and $IFN\gamma^{MUT}_{HLA-pep}$ define interferon gamma response as measured by ELISA assay for the wild-type and mutated antibodies against empty HLA-A2.

The first term in Equation 1 evaluates the difference between theoretical and experimentally observed changes in HLA-A2/peptide-antibody complex stability upon mutation, and the second term evaluates the difference between theoretical and experimentally observed ability of mutation to stabilize interactions between antibody and peptide as compared with the interaction between antibody and HLA-A2.

Evaluation of Allosteric Effects

To evaluate allosteric effects in the scFv/HLA-A2/peptide system, we employed the AlloSigMA server.[23] The effect of three mutations (V_L S31Y, V_L G93L, and V_H G55F) was calculated using the "DOWN-mutated residue" option. This option defines the loosen local contact network. We chose it to describe local

destabilization, which results in decreased binding of scFv to irrelevant MAGEA3-P$_{271-279}$ peptide-loaded HLA-A2 molecules and to empty HLA-A2 molecules. The effect of mutations V$_H$ S100V and V$_H$ S53M was calculated using the "UP-mutated residue" option. This option defines the stiffen local contact network. It was chosen to describe local stabilization, which results in increased binding of scFv to HER2-P$_{369-377}$ peptide-loaded HLA-A2 molecules.

Cell Lines

T2 cells were purchased from American Type Culture Collection (ATCC) and cultured in RPMI1640 medium (GIBCO) supplemented with 10% FBS and 2 mM GlutaMAX. All cell lines were mycoplasma free and validated by flow cytometry for surface markers and functional readouts as needed.

Generation and Characterization of mAb SF2

The mAb SF1 is secreted by a hybridoma generated by fusing mouse myeloma cells P3-X36-Ag8.653 with splenocytes from an 8-week-old female BALB/c mouse immunized with HLA-A2 antigen HER2/neu$_{369-377}$ peptide complexes according to the following schedule. Three days before priming, the 6-week-old female BALB/c mouse was injected intramuscularly with 100 μg (per mouse) of granulocyte-macrophage colony-stimulating factor (GM-CSF) plasmid. Subsequently, the mouse was primed with HLA-A2 antigen HER2/neu$_{369-377}$ peptide complexes (50 μg) utilizing saponin, which can enhance both B cell and T cell response[33] as an adjuvant. Boosters were given at 2-week intervals for a total of 14 times. Four days following the last booster a mouse was sacrificed. Splenocytes were harvested from the immunized mouse and fused to mouse myeloma cells P3-X36-Ag8.653 at a ratio of 1:1 as previously described.[34] Twenty 96-well, flat-bottom microtiter plates (Corning, Corning, NY, USA) were seeded with 1.5–2 × 10^5 cells/well. Growth of colonies was observed in all seeded wells. Supernatants were screened in ELISA with HLA-A2 antigen HER2/neu$_{369-377}$ peptide complexes.

HLA-A2 antigen/MAGE-3$_{271-279}$ peptide complexes and HLA-A2/MART1$_{27-35}$ peptide complexes were used as specificity controls. In the first screening, about 30 hybridomas displayed higher reactivity with HLA-A2 antigen HER2/neu$_{369-377}$ peptide complexes than with the other complexes. In additional screenings, only the hybridoma SF1 maintained its selected reactivity with HLA-A2 antigen HER2/neu$_{369-377}$ peptide complexes. The mAb SF1-stained T2 cells pulsed with the HER2/neu$_{369-377}$ peptide, but not with peptides derived from other tumor antigens.[35] On the other hand, the mAb SF1 did not stain cell lines that expressed both HLA-A2 and HER2/neu.

Plasmid Construction and Retrovirus Production

The variable regions of the V$_H$ and V$_L$ chains of the SF2 mAb were cloned from the SF2 mouse hybridoma. The V$_L$ amino acid sequence was: 1-DIQMTQSPASLSVSVGETVTITCRPSENIYSNLAWYQQK QGKSPQLLVYAATHLADGVPSRFSGSGSGTQYSLKINSLQSEDF GTYYCQHFWGTPYTFGGGTKLEIK-107. CDRs as identified using a previously described set of rules[28] are underlined. The corresponding residue ranges are CDR1 (residues 24–34), CDR2 (residues 49–56), and CDR3 (residues 89–97). The V$_H$ amino acid sequence was: 1-QVQLKQSGPGLLQPSQSLSITCTVSGFSLTSYGVHWVRQS PGKGLEWLGVIWSGGSTDYNAAFISRLSISKDNSKSQFFFKMNS LQIDDTAIYYCATGSSHWYFDVWGAGTTVTVSS-117. CDRs as identified using a previously described set of rules[28] are underlined. The corresponding residue ranges are CDR1 (residues 23–35), CDR2 (residues 50–58), and CDR3 (residues 96–106).

The scFv was created by connecting the C terminus of V$_L$ with the N terminus of V$_H$ using 15-residue peptide linker GGGGSGGG GSGGGGS and then cloned into a previously validated CAR cassette that includes the human CD8α hinge and transmembrane domain, CD28 intracellular costimulatory domains, and CD3ζ intracellular signaling domain.[4] The SF2.CAR cassettes were cloned into the retroviral vector SFG. Mutations of the scFv were created by PCR and were listed as follows: set 1: V$_L$ S31Y (CDR1), N32Y (CDR1), A50L (CDR2), A50F (CDR2), T52Y (CDR2), G93L (CDR3); V$_H$ S28Y (CDR1), T30E (CDR1), S31L (CDR1), G55F (CDR2), S56Y (CDR2), S100M (CDR3); and set 2: V$_L$ N32Q (CDR1), A50V (CDR2), G93I (CDR3), G93V (CDR3); V$_H$ S53M (CDR2), S100V (CDR3), H101I (CDR3). Retroviral supernatants were prepared as previously described.[36]

Transduction and Expansion of Human T Cells

Buffy coats from healthy donors were obtained through the Gulf Coast Regional Blood Center, Houston, TX, USA. Peripheral blood mononuclear cells (PBMCs) isolated with Lymphoprep density separation (Fresenius Kabi Norge) were activated using 1 μg/mL anti-CD3 (Miltenyi Biotec) and 1 μg/mL anti-CD28 (BD Biosciences) mAb-coated plates. On day 3, T lymphocytes were transduced with retroviral supernatants using retronectin-coated plates (Takara Bio, Shiga, Japan). After removal from retronectin plates, T cells were expanded in complete medium (45% RPMI 1640 and 45% Click's medium [Irvine Scientific], 10% FBS [Hyclone], 2 mM GlutaMAX, 100 U/mL penicillin, and 100 μg/mL streptomycin) with IL-7 (10 ng/mL; PeproTech) and IL-15 (5 ng/mL; PeproTech), changing medium every 2–3 days. On days 12–14, cells were collected for *in vitro* co-culture experiments.

Co-culture and ELISA

T cells (5 × 10^5) were co-cultured with T2 cells (5 × 10^5) in a 24-well plate without the addition of exogenous cytokines. After 24 h, supernatants were collected, and IFNγ level was measured by using an ELISA kit (R&D Systems) following the manufacturer's instructions. Each supernatant was measured in duplicate.

Flow Cytometry

The expression of SF2.CAR was detected using anti-Fab antibody (Jackson ImmunoResearch Laboratories). Samples were analyzed with BD FACSCanto II or BD FACSFortessa with the BD Diva software (BD Biosciences); for each sample we

acquired a minimum of 10,000 events, and data were analyzed using FlowJo 10.

SUPPLEMENTAL INFORMATION

Supplemental Information can be found online at https://doi.org/10.1016/j.omto.2019.08.008.

AUTHOR CONTRIBUTIONS

A.K. and K.P. performed molecular dynamics simulations and interpreted the data. H.D. and K.H. performed and interpreted the molecular and immunologic experiments. T.K., X.W., and S.F. generated and provided the antibodies. G.D. and N.V.D. conceptually designed the project and interpreted the data. A.K., H.D., G.D., and N.V.D. wrote the manuscript with contributions from all of the authors.

CONFLICTS OF INTEREST

The authors declare no competing interests.

ACKNOWLEDGMENTS

REFERENCES

1. Smith, G.P. (1985). Filamentous Fusion Phage: Novel Expression Vectors That Display Cloned Antigens on the Virion Surface. Science 228, 1315–1317.

2. Dotti, G., Gottschalk, S., Savoldo, B., and Brenner, M.K. (2014). Design and development of therapies using chimeric antigen receptor-expressing T cells. Immunol. Rev. 257, 107–126.

3. June, C.H., and Sadelain, M. (2018). Chimeric Antigen Receptor Therapy. N. Engl. J. Med. 379, 64–73.

4. Savoldo, B., Ramos, C.A., Liu, E., Mims, M.P., Keating, M.J., Carrum, G., Kamble, R.T., Bollard, C.M., Gee, A.P., Mei, Z., et al. (2011). CD28 costimulation improves expansion and persistence of chimeric antigen receptor-modified T cells in lymphoma patients. J. Clin. Invest. 121, 1822–1826.

5. Almagro, J.C., Teplyakov, A., Luo, J., Sweet, R.W., Kodangattil, S., Hernandez-Guzman, F., and Gilliland, G.L. (2014). Second antibody modeling assessment (AMA-II). Proteins 82, 1553–1562.

6. Almagro, J.C., Beavers, M.P., Hernandez-Guzman, F., Maier, J., Shaulsky, J., Butenhof, K., Labute, P., Thorsteinson, N., Kelly, K., Teplyakov, A., et al. (2011). Antibody modeling assessment. Proteins 79, 3050–3066.

7. Teplyakov, A., Luo, J., Obmolova, G., Malia, T.J., Sweet, R., Stanfield, R.L., Kodangattil, S., Almagro, J.C., and Gilliland, G.L. (2014). Antibody modeling assessment II. Structures and models. Proteins 82, 1563–1582.

8. Yamashita, K., Ikeda, K., Amada, K., Liang, S., Tsuchiya, Y., Nakamura, H., Shirai, H., and Standley, D.M. (2014). Kotai Antibody Builder: automated high-resolution structural modeling of antibodies. Bioinformatics 30, 3279–3280.

9. Dokholyan, N.V., Buldyrev, S.V., Stanley, H.E., and Shakhnovich, E.I. (1998). Discrete molecular dynamics studies of the folding of a protein-like model. Fold. Des. 3, 577–587.

10. Shirvanyants, D., Ding, F., Tsao, D., Ramachandran, S., and Dokholyan, N.V. (2012). Discrete molecular dynamics: an efficient and versatile simulation method for fine protein characterization. J. Phys. Chem. B 116, 8375–8382.

11. Proctor, E.A., and Dokholyan, N.V. (2016). Applications of Discrete Molecular Dynamics in biology and medicine. Curr. Opin. Struct. Biol. 37, 9–13.

12. Comeau, S.R., Gatchell, D.W., Vajda, S., and Camacho, C.J. (2004). ClusPro: a fully automated algorithm for protein-protein docking. Nucleic Acids Res 32, W96–W99.

13. Kozakov, D., Hall, D.R., Xia, B., Porter, K.A., Padhorny, D., Yueh, C., Beglov, D., and Vajda, S. (2017). The ClusPro web server for protein-protein docking. Nat. Protoc 12, 255–278.

14. Rossjohn, J., Gras, S., Miles, J.J., Turner, S.J., Godfrey, D.I., and McCluskey, J. (2015). T cell antigen receptor recognition of antigen-presenting molecules. Annu. Rev. Immunol. 33, 169–200.

15. Gras, S., Chadderton, J., Del Campo, C.M., Farenc, C., Wiede, F., Josephs, T.M., Sng, X.Y.X., Mirams, M., Watson, K.A., Tiganis, T., et al. (2016). Reversed T Cell Receptor Docking on a Major Histocompatibility Class I Complex Limits Involvement in the Immune Response. Immunity 45, 749–760.

16. La Gruta, N.L., Gras, S., Daley, S.R., Thomas, P.G., and Rossjohn, J. (2018). Understanding the drivers of MHC restriction of T cell receptors. Nat. Rev. Immunol. 18, 467–478.

17. Dokholyan, N.V. (2016). Controlling Allosteric Networks in Proteins. Chem. Rev. 116, 6463–6487.

18. Guarnera, E., and Berezovsky, I.N. (2019). On the perturbation nature of allostery: sites, mutations, and signal modulation. Curr. Opin. Struct. Biol. 56, 18–27.

19. Wodak, S.J., Paci, E., Dokholyan, N.V., Berezovsky, I.N., Horovitz, A., Li, J., Hilser, V.J., Bahar, I., Karanicolas, J., Stock, G., et al. (2019). Allostery in Its Many Disguises: From Theory to Applications. Structure 27, 566–578.

20. Papaleo, E., Saladino, G., Lambrughi, M., Lindorff-Larsen, K., Gervasio, F.L., and Nussinov, R. (2016). The Role of Protein Loops and Linkers in Conformational Dynamics and Allostery. Chem. Rev. 116, 6391–6423.

21. Lua, W.-H., Su, C.T.-T., Yeo, J.Y., Poh, J.-J., Ling, W.-L., Phua, S.-X., and Gan, S.K. (2019). Role of the IgE variable heavy chain in FcεRIα and superantigen binding in allergy and immunotherapy. J. Allergy Clin. Immunol. 144, 514–523.e5.

22. Srivastava, A., Tracka, M.B., Uddin, S., Casas-Finet, J., Livesay, D.R., and Jacobs, D.J. (2016). Mutations in Antibody Fragments Modulate Allosteric Response Via Hydrogen-Bond Network Fluctuations. Biophys. J. 110, 1933–1942.

23. Guarnera, E., Tan, Z.W., Zheng, Z., and Berezovsky, I.N. (2017). AlloSigMA: allosteric signaling and mutation analysis server. Bioinformatics 33, 3996–3998.

24. Yusakul, G., Sakamoto, S., Pongkitwitoon, B., Tanaka, H., and Morimoto, S. (2016). Effect of linker length between variable domains of single chain variable fragment antibody against daidzin on its reactivity. Biosci. Biotechnol. Biochem. 80, 1306–1312.

25. Dolezal, O., Pearce, L.A., Lawrence, L.J., Mccoy, A.J., Hudson, P.J., and Kortt, A.A. (2000). ScFv multimers of the anti-neuraminidase antibody NC10: shortening of the linker in single-chain Fv fragment assembled in VL to VH orientation drives the formation of dimers, trimers, tetramers and higher molecular mass multimers. Protein Eng 13, 565–574.

26. Fisk, B., Blevins, T.L., Wharton, J.T., and Ioannides, C.G. (1995). Identification of an immunodominant peptide of HER-2/neu protooncogene recognized by ovarian tumor-specific cytotoxic T lymphocyte lines. J. Exp. Med. 181, 2109–2117.

27. Andersen, H.C. (1980). Molecular dynamics simulations at constant pressure and/or temperature. J. Chem. Phys. 72, 2384–2393.

28. North, B., Lehmann, A., and Dunbrack, R.L., Jr. (2011). A new clustering of antibody CDR loop conformations. J. Mol. Biol. 406, 228–256.

29. Yin, S., Ding, F., and Dokholyan, N.V. (2007). Eris: an automated estimator of protein stability. Nat. Methods 4, 466–467.

30. Yin, S., Ding, F., and Dokholyan, N.V. (2007). Modeling backbone flexibility improves protein stability estimation. Structure 15, 1567–1576.

31. Yin, S., Biedermannova, L., Vondrasek, J., and Dokholyan, N.V. (2008). MedusaScore: an accurate force field-based scoring function for virtual drug screening. J. Chem. Inf. Model. 48, 1656–1662.

32. Yin, S., Ding, F., and Dokholyan, N.V. (2010). Modeling mutations in proteins using Medusa and discrete molecule dynamics. In Introduction to Protein Structure Prediction: Methods and Algorithms, H. Rangwala and G. Karypis, eds. (John Wiley & Sons), pp. 453–476.

33. Schaed, S.G., Klimek, V.M., Panageas, K.S., Musselli, C.M., Butterworth, L., Hwu, W.J., Livingston, P.O., Williams, L., Lewis, J.J., Houghton, A.N., and Chapman, P.B. (2002). T-cell responses against tyrosinase 368-376(370D) peptide in HLA*A0201+ melanoma patients: randomized trial comparing incomplete Freund's adjuvant, granulocyte macrophage colony-stimulating factor, and QS-21 as immunological adjuvants. Clin. Cancer Res. 8, 967–972.

34. Köhler, G., and Milstein, C. (1975). Continuous cultures of fused cells secreting antibody of predefined specificity. Nature 256, 495–497.

35. Wang, X., Campoli, M., Ko, E., Luo, W., and Ferrone, S. (2004). Enhancement of scFv fragment reactivity with target antigens in binding assays following mixing with anti-tag monoclonal antibodies. J. Immunol. Methods 294, 23–35.

36. Vera, J., Savoldo, B., Vigouroux, S., Biagi, E., Pule, M., Rossig, C., Wu, J., Heslop, H.E., Rooney, C.M., Brenner, M.K., and Dotti, G. (2006). T lymphocytes redirected against the κ light chain of human immunoglobulin efficiently kill mature B lymphocyte-derived malignant cells. Blood 108, 3890–3897.